Journal of Alloys and Compounds 582 (2014) 181–185

Contents lists available at ScienceDirect

Journal of Alloys and Compounds

journal homepage: www.elsevier.com/locate/jalcom

Structural stability and electronic structures of (1 1 1) twin boundaries in the rock-salt MnS

Y.B. Xue, Y.T. Zhou, D. Chen *, X.L. Ma *

Shenyang National Laboratory for Materials Science, Institute of Metal Research, Chinese Academy of Sciences, Wenhua Road 72, 110016 Shenyang, China

ARTICLE INFO

Article history:
Received 30 May 2013
Received in revised form 23 July 2013
Accepted 8 August 2013
Available online 20 August 2013

Keywords:
Twin
Rock-salt compounds
TEM
First-principles calculation

ABSTRACT

In the work, we report a theoretical and experimental study of the {1 1 1} twin boundaries in the rock-salt MnS using aberration-corrected transmission electron microscopy (TEM) and density functional theory. The experimental TEM images are supported by first-principle calculations. In comparison with magnesium oxide, we also explained why it is comparatively more stable for twins to exist in MnS rather than in MgO, which may help us better understand the properties of different ionic compounds.

1. Introduction

Over the years, many efforts have been made to understand the effect of twins on metals and ionic compounds at the atomic scale, because the plastic formability is closely related to the ease of the formation of planar defects along the close-packed planes, namely, twin and stacking faults [1]. In metals, it was found that copper samples with a high density of nanoscale twins showed a tensile strength about 10 times higher than that of conventional coarse-grained copper, while retaining an electrical conductivity comparable to that of pure copper [2]. And twin boundaries are effective in enhancing the ductility and fracture toughness of the materials without compromising the high strengths [3,4]. Recently, Singh et al. investigated the effect of twin density on the crack initiation toughness and stable fatigue crack propagation characteristics of nanotwinned copper [5]. Using dynamic plastic deformation method, Yan studied the strength and ductility of 316L austenitic stainless strengthened by nano-scale twin bundles [6]. As for ionic compounds with rock-salt structure, the twin boundaries have been not only observed experimentally through diffraction experiments and transmission electron microscopy [7,8], but also been calculated by theoreticians to explore their electronic structures and energetics [9,10].

MnS can exist in three allotropic modifications: the rock-salt structure α-MnS, zinc-blende structure β-MnS and wurtzite structure γ-MnS [11]. The α-MnS is a stable rock-salt structure at ambient temperature and pressure conditions, which is the main object of this work. In recent decades, MnS has received considerable attention not only in the field of functional materials, due to its unique magneto-optical and electronic properties [11,12], but also in the field of structural materials, due to its important role in pitting corrosion of austenitic stainless steels [13] and its lubricating effect that is needed for machining. On the one hand, MnS belongs to the family of diluted magnetic semiconductors with potential applications in light-emitting devices, photo-detectors, solar cells, etc. Pioneer works on MnS have been devoted to the controllable synthesis of nanocrystals [11], the identification of the high-pressure structural transition [14], and the investigation of the magneto-optical properties [12]. On the other hand, MnS is a very common inclusion in steels, with great influence on the pitting corrosion [13] and mechanical property of stainless steels. To the best of our knowledge, little attention has been paid to the MnS twins which may have relevance to the property of materials. In this work, the structures of twin boundaries in the rock-salt MnS are studied by aberration-corrected transmission electron microscopy and first-principles calculations, which is expected to provide a new understanding of such defects in rock-salt compounds.

2. Experimental and calculation methods

Microstructure characterization of twin structures were performed at 300 kV using a Titan G60-300 TEM equipped with double spherical aberration (Cs) correctors for both the probe-forming and image-forming lenses. The convergent semiangle was chosen as 20.8 mrad, and a large inner collection angle was set as 50 mrad. The composition of the stainless steel in the present study is shown in Table 1. We choose 316F stainless steel because it provides a large number of MnS inclusions for analysis. This steel sample was made by Nippon Steel and Sumikin Stainless Steel Corporation [15]. The steel sample was hot-rolled (>1000 °C) into rods with diameter of 1 cm.

* Corresponding authors. Tel.: +86 24 83978629 (D. Chen).
E-mail addresses: dchen@imr.ac.cn (D. Chen), xlma@imr.ac.cn (X.L. Ma).

0925-8388/$ - see front matter © 2013 Elsevier B.V. All rights reserved.
http://dx.doi.org/10.1016/j.jallcom.2013.08.073

Table 1
Compositions of the 316F stainless steel in the present study (The compositions are expressed as weight percent.).

S	C	Cr	Ni	Mn	Mo	Co	V
0.16	0.04	16.68	10.07	1.60	2.15	0.13	0.09
Ti	Cu	Si	P	Al	Nb	Sn	Fe
<0.005	0.26	0.46	0.030	0.06	0.04	0.001	Balance

All calculations were carried out with the Vienna *Ab initio* Simulation Package (VASP) [16,17] in the framework of density functional theory (DFT). We adopted the projector-augmented wave (PAW) method [18,19] to describe the core–valence electron interaction and the generalized gradient approximation (GGA) formulated by Perdew, Burke and Ernzerhof (PBE) [20] was employed to treat the exchange correlation between electrons. The Mn 3p, 3d and 4s, S 3s and 3p, Mg 2s, O 2s and 2p orbitals were chosen as valence states. Spin polarization was allowed for MnS, but not for MgO. The plane-wave cutoff energy was set at 450 eV and 400 eV for MnS and MgO, respectively. A conjugate-gradient algorithm was used to relax the ions into their equilibrium positions and the total energy was obtained when it converged to 10^{-4} eV in the electronic self-consistent loop. The Monkhorst–Pack scheme [21] was used for the *k*-point sampling and the Brillouin zone integration was performed with the tetrahedron method with Blöchl corrections [22,18]. Highly converged results were obtained utilizing $5 \times 5 \times 1$ *k*-point grid for both MnS and MgO twin models.

As a benchmark test for our approach and parameterization, we first investigated the ground-state properties of the perfect bulk MnS and MgO. A series of total energies were calculated as a function of the unit-cell volume and then fitted to the Murnaghan [23] equation of state. The optimized lattice parameters (a_{MnS} = 5.110 Å and a_{MgO} = 4.237 Å) are very close to the experimental values (a_{MnS} = 5.224 Å and a_{MgO} = 4.220 Å), listed in the sixth column of Table 2, so they can be safely adopted to build the twin models.

3. Results and discussion

3.1. Structural determination and stability analysis of MnS twins

In our TEM studies, we identified that MnS inclusions were deformed by dislocation and twinning when steel matrix experienced hot-rolling. Fig. 1(a) shows a low magnification image of an elongated MnS inclusion, where several deformation twins are obviously observed. The inset displays the corresponding selected-area-diffraction (SAD) pattern, in which the twin relationships are represented by two rectangles consisting of diffraction

Table 2
Properties of bulk MnS, MgO and their twins: twin boundary energy ζ (mJ/m^2); interplanar distance between twin boundary and its nearest (1 1 1) plane d1 (Å), refer to Fig. 1, quantities in parenthesis are the rate of change; electron transfer number Δn (negative sign means losing electrons, positive sign means receiving electrons); elecronegativity χ (in Pauling scale); unit cell lattice constant a_0 (Å) from calculation (calc.) and experiment (exp.).

	ζ	d1	Δn	χ	a_0
Bulk-MnS		1.476	Mn: − 1.146 ***e*** S: + 1.164 ***e***	Mn:1.55	5.110 calc.
Twin-S	81	1.489 (0.88%)	Mn:−1.130 ***e*** S: + 1.109 ***e***	S:2.58	5.224 exp. [24]
Twin-Mn	481	1.578 (6.91%)	Mn: − 1.081 ***e*** S: + 1.148 ***e***	($\Delta\chi$ = 1.03)	
Bulk-MgO		1.223	Mg: − 2.000 ***e*** O: + 2.000 ***e***	Mg:1.31	4.237 calc.
Twin-Mg	661	1.277 (4.41%)	Mg: − 2.000 ***e*** O: + 2.000 ***e***	O:3.44	4.220 exp. [25]
Twin-O	1034	1.295 (5.89%)	Mg: − 2.000 ***e*** O: + 2.000 ***e***	($\Delta\chi$ = 2.13)	

spots from twins and matrices. The twin plane is {1 1 1} plane, which is the most common twin plane in the rock-salt compounds. To provide insight into the structural details of twins in MnS, the high-angle-angular-dark-field (HAADF) scanning TEM (STEM) technique, which provides strong contrast associated with the atomic number 'Z' of the local composite [26], were performed. In Fig. 1(b), the atomic structure of the twin boundary along the [1 1 0] direction is shown, in which the brighter dots correspond to the manganese columns. It is seen that the twinning involves a sulfur {1 1 1} plane as the boundary plane (Twin-S).

As mentioned above, a number of Twin-S has been observed in experiment. To corroborate this phenomenon, we theoretically extracted the twin boundary energy, ζ, by [1].

$$\zeta = (E_{twin} - E_{bulk})/2A \quad (1)$$

where E_{twin} is the total energy of the twin model, E_{bulk} is the total energy of corresponding perfect bulk rock-salt MnS scaled to the supercell size, A is the interfacial area, and the number 2 means that there are two twin boundaries in the supercell model due to the periodic boundary conditions as implemented in our first-principles

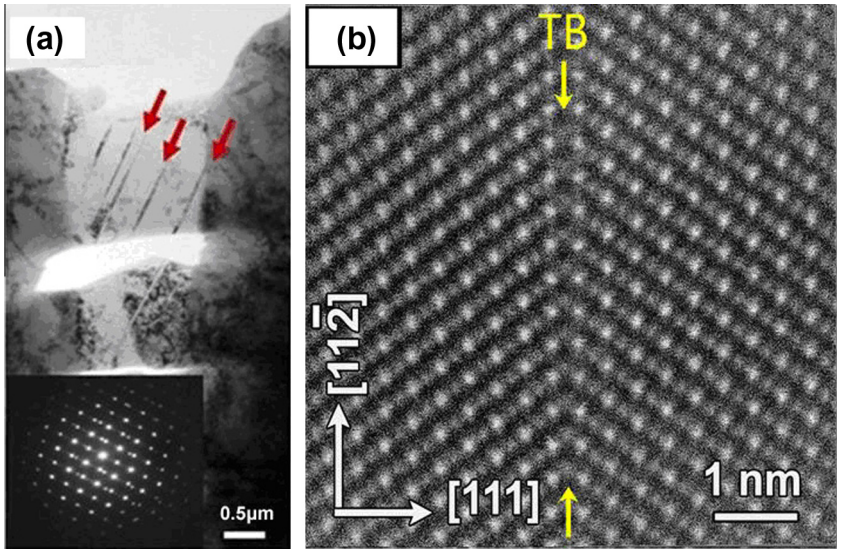

Fig. 1. (a) Low magnification TEM image of MnS inclusion in stainless steel. Twins within MnS inclusion are marked by arrowheads. (b) High resolution STEM image of twin boundary. Note that the Mn columns are brighter than S columns due to their high atom number.

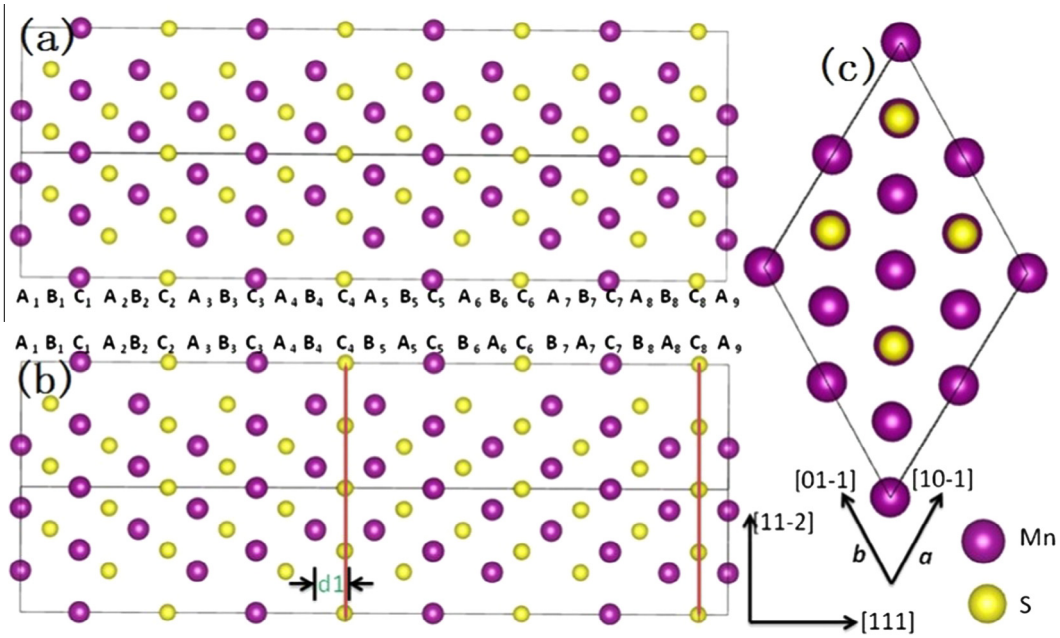

Fig. 2. Twin-X (X = Mn, S, Mg and O) denotes the model where the twin boundaries are occupied by the X ions; Ai (Bi or Ci) denotes the ***i*th** A (B or C) type (1 1 1) plane; d1 means the interplanar distance between twin boundary and its nearest (1 1 1) plane. Examples of structure models are given above: (a) Bulk-MnS; (b) Twin-S, twin boundaries are marked by red lines; (c) side view. (For interpretation of the references to colour in this figure legend, the reader is referred to the web version of this article.)

calculations, see Fig. 2. Because it is possible for both cations and anions to occupy the twin boundary, there are two kinds of {1 1 1} twin models. For simplicity, we defined some symbols to represent them and other objects, such as Twin-Y (Y = Mn, S, Mg and O), Bulk-X (X = MnS, MgO), A_i (B_i or C_i), and d1 refer to Fig. 2 for their meanings. The calculated twin boundary energies are summarized in the second column in Table 2. With the twin boundary energy calculated for different structure configurations, we can analyze the relative stability of different twin structures. The smaller the twin boundary energy, the more stable the atomic structure of twin boundary. Expectedly, ζ (Twin-S) is indeed considerably lower than ζ (Twin-Mn), which suggests that Twin-S is preferred from an energetic standpoint, in good agreement with experimental observations.

As a rule of thumb, twin boundary energy is closely associated with the atomic arrangement therein, so we carefully analyzed the atomic structures of these two twin boundaries so as to get insight into the cause for the differences between ζ (Twin-S) and ζ (Twin-Mn). The results are shown in the third columns in Table 2. Apparently, d1(Twin-Mn) is significantly larger than d1(bulk-MnS), by contrast, d1(Twin-S) is very close to d1(bulk-MnS), which suggests there exists strong repulsive force among (1 1 1) planes near the twin boundary for Twin-Mn, whereas the repulsive force becomes much weaker for Twin-S. At this very moment we may ascribe the differences in twin boundary energies to the different levels of (1 1 1) interplanar expansions near the twin boundary. Nonetheless, it is still necessary for us to find out where the repulsive force comes from.

In order to elucidate this issue, we take into consideration the change in the atomic configurations between the bulk and twin structures and its effect on the interatomic interaction. As is well known, twins are a kind of planar defect and the modification of coordination geometry happens only at the twin boundary. As for MnS twins, there are always six nearest neighbor atoms for each atom, but at the twin boundary the arrangement of the six atoms changes into a triangular prism from an octahedron, see Fig. 3(a) and (b). In this work, the ions can be treated as point charge approximately. If ions are invariant and have same signs of charges, the repulsive force will be inversely proportional to the square of the distance according to Coulomb's law equation. In Fig. 3(a) and (b), d2 (triangular prism) (2.95 Å) is shorter than d2 (octahedron) (3.62 Å), so the repulsive force would be stronger with twin structure in Fig. 3(b). Moreover, the ionic radius of anion S is longer than that of cation Mn which causes the more superposition of S–S electronic density, as shown in Fig. 3(c) and (d). It means that the electrostatic force could be further enhanced when the triangular prism consist of anion S.

To further explore the electronic structures of MnS twins, the electronic density isosurfaces for Twin-Mn and Twin-S are respectively shown in Fig. 3(e) and (f). In Fig. 3(e), it was found that the Mn-S electronic density overlaps comparatively less at the twin boundary, indicating the covalent bonds between them turn to be weaker in Twin-Mn. In Fig. 3(f), the electronic density distributes symmetrically on both sides of twin boundary and overlaps similarly to that away from the boundary, indicating the strength of S-Mn covalent bonds has not changed at Twin-S boundary. As a result, d1(Twin-Mn) should be larger than d1(Twin-S) which corresponds with data listed in the third column of Table 2. Therefore, the favorable Twin-S may be due to the following explanations: (1) the electrostatic force dominates in the expansion of (1 1 1) planes at the twin boundary, (2) incomplete Mn-S covalent bonds increase the twin boundary energy further.

3.2. Differences between MnS and MgO

It is well known that solid magnesium oxide is a textbook example of typical ionic compounds with rock-salt structure. So, comparative studies between MnS and MgO may capture a lot of interest in the field although there are no experimental data available for MgO.

As mentioned above, the twin boundary energy is closely related to the interatomic repulsion, so we firstly pay our attention to the differences in their intrinsic properties, such as chemical

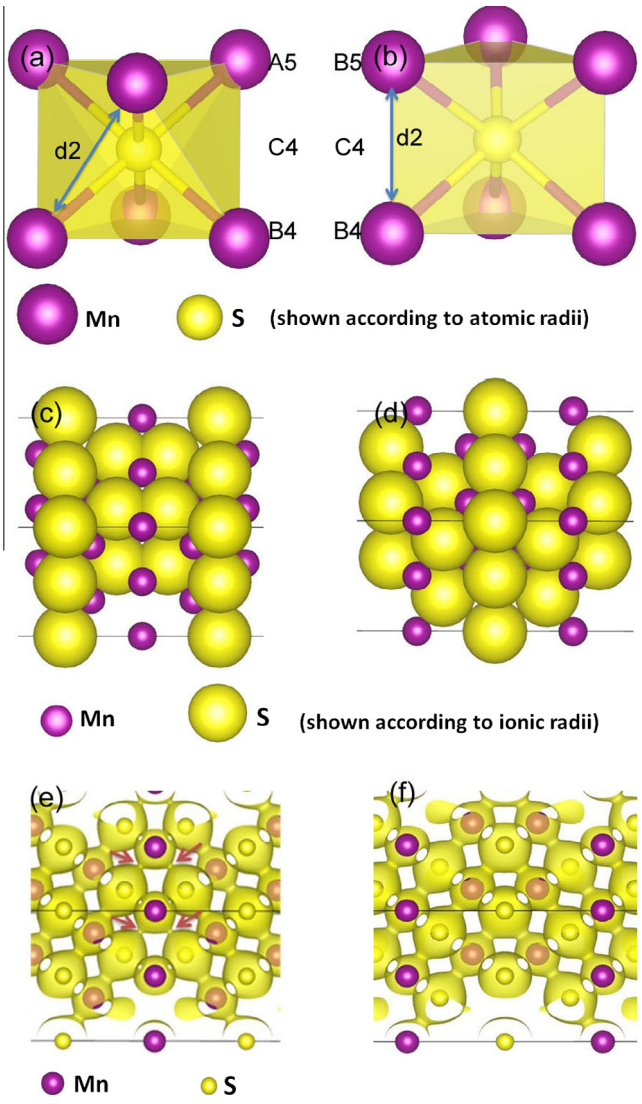

Fig. 3. Atomic and electronic structures for MnS twins (only the fragments near twin boundary are given). (a) and (b) The examples of the coordination geometry of S atoms in bulk and at the twin boundary, respectively, in which the double-headed arrow stands for the nearest distance of the same kind of atoms between two (1 1 1) planes (d2). (c) and (d) Another representation of Twin-Mn and Twin-S, where atoms are rendered with their ionic radii. (e) and (f) Isosurfaces of charge density for Twin-Mn and Twin-S, which are depicted at 0.04 e/Å^3. All structures are visualized using VESTA code [27].

bonds and elemental characteristics. Fig. 4(a) and (b) are shown the charge density differences of (0 0 1) planes for perfect bulk MnS and MgO, respectively, which qualitatively represent the redistribution of their valence electrons. Clearly, the electrons transferred from Mn to S, redistributing not very uniformly. More electrons existed in between S and Mn, but came nearer to S, indicating the formation of polar bonds. And the interaction between S and S can even be found in the picture. By contrast, in the MgO, the valence electrons redistributed around O atoms spherically and homogeneously, which is the characteristics of standard ionic bonds. As an intuitive scheme for visualizing atoms in molecules, Bader's definition of an atom is based purely on the electronic charge density, which is often useful for charge analysis. In the work, following the Bader charge analysis approach coded by Henkelman and coworkers [28,29], we calculated quantitatively the net gain and loss of valence electrons on each atom in perfect bulk MnS and MgO. The results are listed in the fourth column of Table 2, which clearly show that Mn, S, Mg and O are in charge states of + 1.146, −1.146, + 2.000 and −2.000, respectively. Remarkably, the results for MnS are smaller in magnitude than their conventional oxidation states defined in inorganic chemistry (Mn^{2+} and S^{2-}), which could be attributed to the not big enough difference in electronegativity between Mn and S ($\Delta\chi$ = 1.03) with respect to the big one between Mg and O ($\Delta\chi$ = 2.13). By contrasting MnS with MgO, it can be obtained that MgO is more ionic than MnS, which indicates that the electrostatic repulsion of O–O (Mg–Mg) is larger than that of S–S (Mn–Mn) at the twin boundary.

Next, let us turn our focus to their twins to trace more information. Following the previous method, we calculated the corresponding properties of twins for MgO and added them to Table 2. The most outstanding feature of MgO is that both Twin-Mg and Twin-O have very high values of twin boundary energy (ζ), which indicates that the MgO twins might exist unfavorable and would be difficult to detect experimentally. Given the more-charged ions and the shorter lattice parameters in MgO with respect to MnS, we can readily argue that, for MgO twins, there are very strong repulsive electrostatic forces between atoms in the triangular prism geometry, which results in the much higher ζ and larger d1. As for the electronic structures of MgO twins (not shown here), no matter it is at the twin boundary or elsewhere, the electronic density distributes spherically around each ion as in the bulk MgO, because the ionic bonds exist very strong.

3.3. Effect of [1 1 1] strain on MnS twins

In addition, we particularly make an effort to analyze the effect of the strain on the stability of MnS twins. During the calculation, the total volume of the interfacial area is fixed and the [1 1 1] strain just changed the (1 1 1) interplanar distance in the two twin models (Twin-Mn and Twin-S). As mentioned before, (1 1 1) planes near the twin boundary repel each other, which suggests that [1 1 1] strain may have significant impact on the energetics of the bulk and the twins. Hence, diagrams of twin boundary energy vs. [1 1 1] strain have been drawn in Fig. 5. As we can see in Fig. 5(b), the twin boundary energy of Twin-S decreased as the compressive strain increased, and it would reach nearly half as much as the original value when the compressive strain became 5%. By contrast, the twin boundary energy of Twin-Mn decreased when the tensile strain increased, and it would reach the minimum in Fig. 5(a) when the tensile strain became 5%. However, even so the minimum value is still excessively higher than any value of Twin-S in Fig. 5(b). Consequently, we deduce that [1 1 1] compressive strain may facilitate the stability of Twin-S in MnS.

4. Conclusions

In the rock-salt MnS, Twin-S is a preferred twin structure confirmed both experimentally and theoretically. Based on the first-principles calculations, the structural stability and electronic properties of (1 1 1) twins have been investigated, and the results can be summarized as followings:

(1) Appropriate ionic arrangement leads to lower twin boundary energy of Twin-S than that of Twin-Mn.
(2) For Twin-Mn, at the twin boundary, the strong electrostatic repulsive force and the weaker covalent bonds would cause ξ(Twin-Mn) much higher than ξ(Twin-S).
(3) Substantially strong electrostatic repulsive forces make the existence of MgO twins unfavorable.
(4) Compressive strain along [1 1 1] direction may favor the stabilization of Twin-S in MnS.

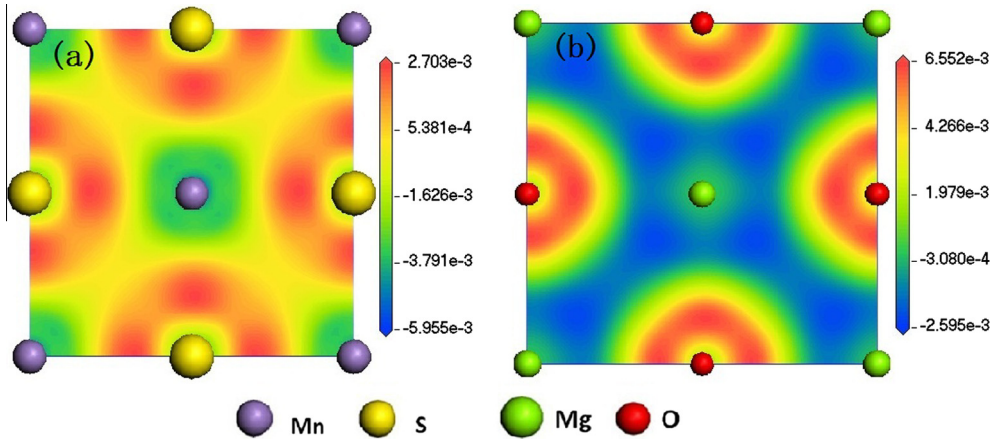

Fig. 4. Charge density difference (in arbitrary units) viewed in the (001) plane for bulk MnS (a) and MgO (b). Charge density decreases most in the dark blue area, increases most in the deep red area and changes moderately elsewhere. (For interpretation of the references to colour in this figure legend, the reader is referred to the web version of this article.)

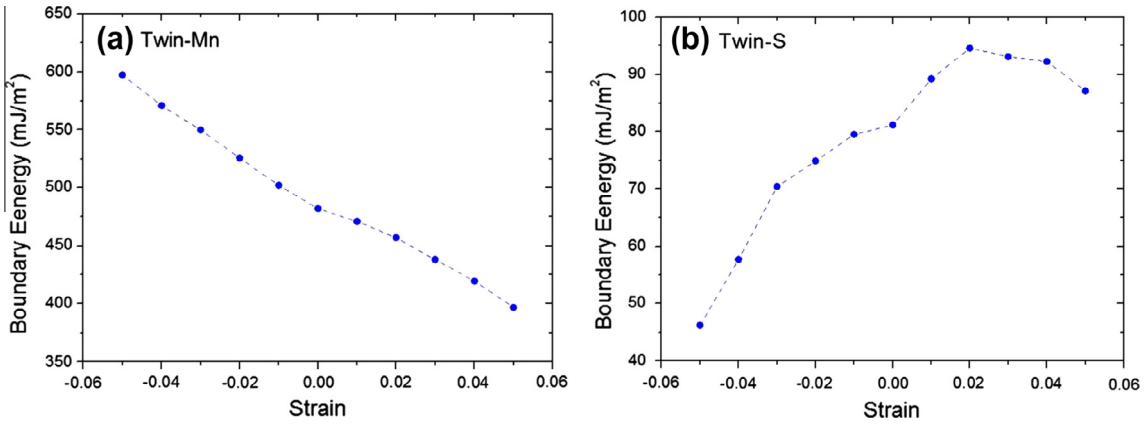

Fig. 5. Calculated twin boundary energy of Twin-Mn (a) and Twin-S (b) as a function of [1 1 1] strain.

Acknowledgment

This work is supported by the Ministry of Science & Technology of China (2009CB623705).

References

[1] Y. Wang, L.Q. Chen, Z.K. Liu, S.N. Mathaudhu, Scripta Mater 62 (2010) 646–649.
[2] L. Lu, Y. Shen, X. Chen, L. Qian, K. Lu, Science 304 (2004) 422–426.
[3] A. Datta, A. Srirangarajan, U.V. Waghmare, U. Ramamurty, A.C. To, Comput. Mater. Sci. 50 (2011) 3342–3345.
[4] K. Lu, L. Lu, S. Suresh, Science 324 (2009) 349–352.
[5] A. Singh, L. Tang, M. Dao, L. Lu, S. Suresh, Acta Mater. 59 (2011) 2437–2446.
[6] F.K. Yan, G.Z. Liu, N.R. Tao, K. Lu, Acta Mater. 60 (2012) 1059–1071.
[7] J.F. Hamilton, L.E. Brady, J. Appl. Phys. 29 (1958) 994.
[8] C.R. Berry, D.C. Skillman, J. Appl. Phys. 33 (1962) 1900–1901.
[9] Z. Ikonic, G.P. Srivastava, J.C. Inkson, J. Phys. Chem. Solids 62 (2001) 579–584.
[10] R.C. Baetzold, J. Phys. Chem. Solids 57 (1996) 627–634.
[11] L. Peng, S. Shen, Y. Zhang, H. Xu, Q. Wang, J. Colloid. Interface Sci. 377 (2012) 13–17.
[12] R. Tappero, P. Wolfers, A. Lichanot, Chem. Phys. Lett. 335 (2001) 449–457.
[13] S.J. Zheng, Y.J. Wang, B. Zhang, Y.L. Zhu, C. Liu, P. Hu, X.L. Ma, Acta Mater. 58 (2010) 5070–5085.
[14] W.Q. Yang, X.H. Zhu, Z.R. Wei, D.Y. Yang, L.Z. Li, Mol. Phys. 109 (2011) 251–256.
[15] <http://www.ns-sc.co.jp/english/seihin/bousen.html>.
[16] G. Kresse, J. Furthmuller, Comput. Mater. Sci. 6 (1996) 15–50.
[17] G.M. Zhang, A.C. Hewson, Phys. Rev. B 54 (1996) 1169–1186.
[18] P.E. Blochl, O. Jepsen, O.K. Andersen, Phys. Rev. B 49 (1994) 16223–16233.
[19] G. Kresse, D. Joubert, Phys. Rev. B 59 (1999) 1758–1775.
[20] J.P. Perdew, K. Burke, M. Ernzerhof, Phys. Rev. Lett. 77 (1996) 3865–3868.
[21] H.J. Monkhorst, J.D. Pack, Phys. Rev. B 13 (1976) 5188–5192.
[22] O. Jepson, O.K. Anderson, Solid State Commun. 9 (1971) 1763–1767.
[23] F.D. Murnaghan, Proc. Natl. Acad. Sci. 30 (1944) 244–247.
[24] J.S. Sweeney, D.L. Heinz, Phys. Chem. Miner 20 (1993) 63–68.
[25] P. Karen, A. Kjekshus, Q. Huang, V.L. Karen, J. Alloys Comp. 282 (1999) 72–75.
[26] S.J. Pennycook, Adv. Imag. Elect. Phys. 123 (2002) 173–206.
[27] K. Momma, F. Izumi, J. Appl. Crystallogr. 41 (2008) 653–658.
[28] G. Henkelman, A. Arnaldsson, H. Jónsson, Comput. Mater. Sci. 36 (2006) 354–360.
[29] W. Tang, E. Sanville, G. Henkelman, J. Phys. Condens. Matter. 21 (2009) 084204.